

Electronic Finetuning of a Bio-inspired Iron(II) tetra-NHC Complex by *trans* Axial Isocyanide Substitution

Jonas F. Schlagintweit⁺, Carolin Hintermeier⁺, Markus R. Anneser, Eva-Maria H. J. Esslinger, Stefan Haslinger, and Fritz E. Kühn*^[a]

Abstract: The synthesis of *trans* axially substituted mono- (1a) and bis(*tert*-butylisocyanide) (1b) derivatives of the highly active homogeneous bio-inspired iron(II) olefin epoxidation (pre-)catalyst 1 bearing an equatorial macrocyclic tetra-*N*-heterocyclic carbene and two *trans* axial labile acetonitrile ligands is reported. NMR spectroscopy and SC-XRD indicate a considerable π -backdonation from the iron(II)

centres to the isocyanide ligand(s). The impact of isocyanide substitution on the electronic features of the complexes is studied by cyclic voltammetry revealing a significant increase in half-cell potential assignable to the reversible Fe(II)/Fe(III) redox couple with an increasing number of isocyanides as a result of their π -accepting properties: $E_{1/2} = 0.15$ V (1), $E_{1/2} = 0.35$ V (1a), $E_{1/2} = 0.44$ V (1b).

Introduction

Iron is the most abundant transition metal in earth's crust (4.7 wt%)^[1] and due to its low toxicity, environmentally friendly features and relatively low price, a very promising candidate for the development of sustainable catalysts.^[2] Unstable metal prices and declining resource stocks^[2b,c,3] have underlined the increased significance of iron compounds over the last years.^[4] Within the last two decades, the mimicking of iron-based enzymes capable of selective oxidation of various organic substrates has gained attention.^[5] A structural motive underlying these natural complexes like heme B or cytochrome P450, are polydentate (mainly tetradentate) *N*-donor ligands, coordinating Fe(II) and Fe(III) centres.^[6]

The successful application of *N*-heterocyclic carbenes (NHCs) as useful ligands to a broad range of transition metal-catalysed reactions^[7] led to the synthesis of bio-inspired iron complexes bearing tetradentate NHC ligands such as 1 and 2 (Figure 1).^[8] 1 and 2 have been applied successfully as catalyst precursors for oxidation catalysis and enable the challenging CH oxidation of alkanes and aromatic compounds, as well as the epoxidation of olefins.^[1,8a,9] 1 and its Fe(III) derivative in particular show exceptional activity in olefin epoxidation catalysis (unprecedented turnover frequencies up to 183,000 h⁻¹),^[1] while simultaneously reaching comparably

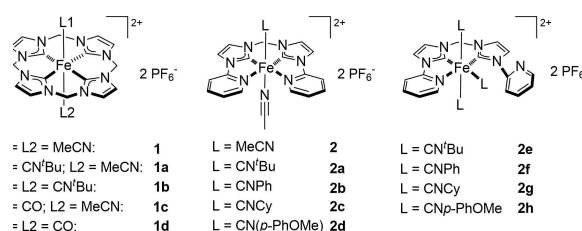


Figure 1. Structures of iron(II) complex 1, its mono- and bis(*tert*-butylisocyanide) substituted derivatives 1a and 1b and their isolobal carbonyl analogues 1c and 1d bearing tetradentate macrocyclic NHC ligand cCCCC (left).^[8b] Structures of iron(II) complexes 2 and 2a–2d bearing tetradentate bis(pyridyl-NHC) ligand NCCN and one isocyanide ligand (middle) and 2e–2h bearing tridentate NCCN and three isocyanide ligands (right).^[8a,10]

high turnover numbers (TON up to 4,300).^[5b] As demonstrated for 2, the substitution with one (Figure 1, middle) or three π -accepting isocyanide ligands (Figure 1, right) significantly impacts the electronic and catalytic properties of the complex, enabling a considerable improvement of the catalyst stability and selectivity in the challenging CH oxidation of alkanes.^[10] The substituent of the isocyanide ligand, *i.e.* *tert*-butyl (^tBu), cyclo-hexyl (Cy), benzyl (Bn), phenyl (Ph) and *para*-methoxyphenyl (*p*-PhOMe), barely impacts the catalytic performance and electronic features as demonstrated by cyclic voltammetry (CV).^[10] However, the amount of coordinating isocyanide ligands (one: 2a–2d vs. three: 2e–2h) has a considerable influence.^[10] Derivatives of 2 bearing two isocyanide ligands could not be isolated. Instead, one of the pyridyl moieties dissociates and is replaced by a third isocyanide ligand, when 2 is reacted with an excess of the latter (Figure 1, right).^[10]

Due to the simple and effective tuning of the electronic features and catalytic performance of 2 by isocyanide substitution,^[10] the same approach is applied to 1, which is significantly more active than 2 in epoxidation catalysis.^[1,9a] The synthesis of mono- (1a) and bis(*tert*-butylisocyanide) (1b) substituted derivatives of 1 are reported (Figure 1, left) in this work. Both compounds are characterised by NMR-spectroscopy, elemental analysis, ESI-MS and single crystal X-ray diffraction

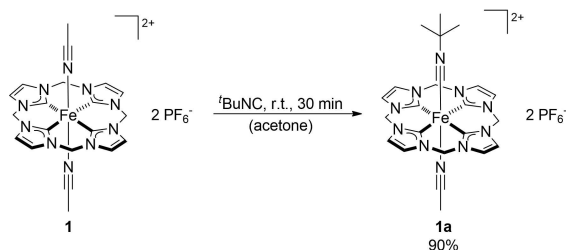
[a] J. F. Schlagintweit,⁺ C. Hintermeier,⁺ Dr. M. R. Anneser, E.-M. H. J. Esslinger, Dr. S. Haslinger, Prof. Dr. F. E. Kühn
Molecular Catalysis, Catalysis Research Center and Department of Chemistry Department
Technische Universität München
Lichtenbergstrasse 4, D-85748 Garching bei München (Germany)
E-mail: fritz.kuehn@ch.tum.de

[⁺] These authors contributed equally to this work.

Supporting information for this article is available on the WWW under <https://doi.org/10.1002/asia.202000214>

© 2020 The Authors. Published by Wiley-VCH Verlag GmbH & Co. KGaA. This is an open access article under the terms of the Creative Commons Attribution Non-Commercial NoDerivs License, which permits use and distribution in any medium, provided the original work is properly cited, the use is non-commercial and no modifications or adaptations are made.

(SC-XRD). In addition, the impact of the π -accepting t BuCN ligand(s) on the electronic properties is studied by cyclic voltammetry and compared to the state-of-the-art iron-based epoxidation (pre-)catalyst **1** and their respective isolobal carbonyl analogues **1c** and **1d**, which been reported previously and are obtained by reacting **1** with carbon monoxide at different temperatures and pressures.^[8b,10] All iron NHC complexes applied in olefin epoxidation show a correlation between their redox potential and catalytic activity, *i.e.* a lower half-cell potential of the reversible Fe(II)/Fe(III) redox couple results in a higher activity.^[1,8c,9a] However, no trend regarding the stability is observed for complexes with different ligand structures. The only correlation between redox potential and turnover number known to date has been described above for complexes bearing the same spectator NHC ligand NCCN, showing a significantly higher TON of **2a–2d** compared to **2**.^[10] Therefore, the obtained CV data of **1a** and **1b** can be used to estimate their potential applicability in (ep-)oxidation catalysis.



Scheme 1. Synthesis of mono(*tert*-butylisocyanide) substituted complex [Fe(cCCCC)(CN t Bu)(MeCN)](PF $_6$) $_2$ **1a**.

Results and Discussion

Synthesis and characterisation of mono(*tert*-butylisocyanide) substituted iron(II) tetra-NHC **1a**

In order to synthesize a mono-isocyanide derivative of **1** a similar approach reported to the modification of **2** is applied.^[10] *tert*-Butylisocyanide (CN t Bu) is chosen due to its simple accessibility and for a better comparison to **2a** and **2e**.

The reaction of **1** with one equivalent CN t Bu in the weakly coordinating solvent acetone at room temperature results in a fast colour change from yellow to emerald green back to a bright yellow. Addition of diethyl ether affords mono-substituted isocyanide complex **1a** in 90% yield (Scheme 1).

The 1 H-NMR of **1a** (Figure 2, top) shows a singlet with a chemical shift of 7.75 ppm and a relative integral of 8 assignable to the backbone protons. In comparison to **1** (7.57 ppm; Figure 2, bottom) the signal is significantly low field shifted (0.18 ppm; Figure 2, middle) as a result of the π -accepting axial isocyanide substituent, which decreases the electron density of the iron centre. As expected, in contrast to **1**, which exhibits one distinct singlet for the methylene protons with a chemical shift of 6.29 ppm in 1 H-NMR due to a fast inversion of the ligand at room temperature, the methylene protons of **1a** show two doublets with relative integrals of 4 each at 6.60 ppm and 6.48 ppm and coupling constants of 12.6 Hz, which is in the typical range of geminal couplings (see SI, Figure 2). The splitting is a result of a loss in symmetry in the equatorial plane as axial ligands are no longer identical (apparent D $_{4h}$ in **1** to apparent C $_{4v}$ in **1a** at room temperature in NMR).

The 13 C-NMR spectrum shows a carbene resonance at 198.9 ppm, which is in the typical range of iron(II) NHC complexes (see SI, Figure 3).^[8,10–11] The signal is significantly high-field shifted compared to compound **1** (205.1 ppm).^[8b] A similar shift has also been reported for mono-isocyanide substituted compounds **2a** and **2c**.^[10] In agreement with other

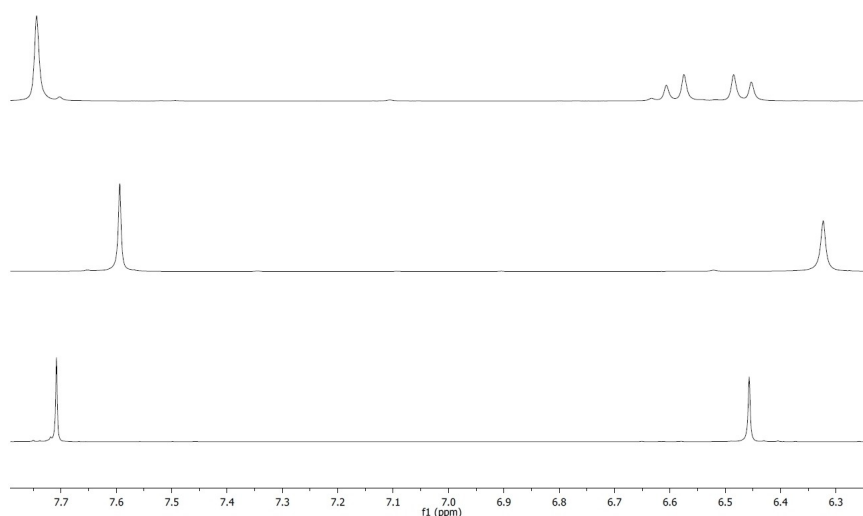


Figure 2. Section of 1 H-NMR spectra of **1a** (top) and **1b** (bottom) in comparison to **1** (middle).

transition metal isocyanide complexes, no resonance corresponding to the coordinating isocyanide carbon atom is observed in the ^{13}C -NMR spectrum, as a result of coupling with ^{14}N and a high relaxation time.^[10,12]

In addition, **1a** was characterised by SC-XRD. Suitable single crystals were obtained by slow vapour diffusion of Et_2O into a solution of **1a** in MeCN. As expected, the iron(II) centre is coordinated in a distorted octahedral fashion (Figure 3).

The $\text{Fe}-\text{C}_{\text{carbene}}$ distances of 1.901(3) Å to 1.913(3) Å are within range of other iron(II) NHC complexes and remain almost unchanged in comparison to the starting material **1**.^[8,11,13] The $\text{Fe}-\text{C}_{\text{isocyanide}}$ distance of 1.819(3) Å is significantly shorter than in compounds **2a–2d** (1.847 Å to 1.852 Å). Due to the similar coordination geometry of **1a** and **2a–2d**, *i.e.* iron(II) in an octahedral environment with an equatorial tetradentate ligand and an acetonitrile ligand *trans* to the isocyanide, this observation is mainly attributable to the influence of the tetradentate ligand. As NHCs are considered to be significantly stronger σ -donors than pyridines,^[14] the tetra-NHC ligand cCCCC increases the electron density of the iron centre in comparison to bis(pyridyl-NHC) ligand NCCN coinciding with a considerably lower reported half-cell potential of **1** in comparison to **2** ($E_{1/2} = 0.15\text{ V vs. } 0.86\text{ V}$),^[8a,b] thus resulting in stronger π -backbonding from the Fe centre to the isocyanide ligand. Therefore, the $\text{Fe}-\text{C}_{\text{isocyanide}}$ bond length is shortened. The $\text{Fe}-\text{N}_{\text{MeCN}}$ distance of 1.974(2) Å is significantly elongated in comparison to those of complex **1** (1.930 Å and 1.933 Å), presumably as a result of the *trans* influence of the CN^tBu ligand. The same trend has been

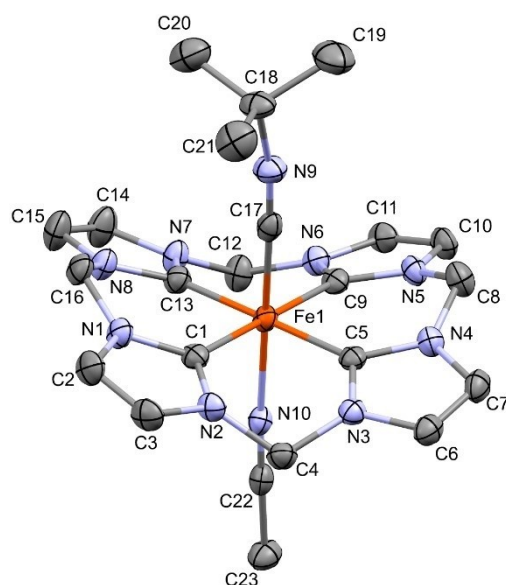


Figure 3. ORTEP-style representation of the cationic fragment of compound **1a**. Hydrogen atoms, co-crystallized solvent molecules and hexafluorophosphate anions are omitted for clarity. Thermal ellipsoids are shown at a 50% probability level. Selected bond lengths (Å) and angles (°): Fe1–C1 1.902(3), Fe1–C5 1.901(3), Fe1–C9 1.913(3), Fe1–C13 1.904(3), Fe1–C17 1.819(3), Fe1–N10 1.974(2), C17–Fe1–C5 90.45(11), C17–Fe1–C1 87.33(11), C5–Fe1–C1 90.34(11), C17–Fe1–C13 90.11(11), C5–Fe1–C13 179.44(11), C1–Fe1–C13 89.66(11), C17–Fe1–C9 93.04(11), C5–Fe1–C9 89.77(11), C1–Fe1–C9 179.61(11), C13–Fe1–C9 90.23(11), C17–Fe1–N10 177.95(10), C5–Fe1–N10 88.34(10), C1–Fe1–N10 91.02(10), C13–Fe1–N10 91.10(10), C9–Fe1–N10 88.61(10), N9–C17–Fe1 176.6(2), C17–N9–C18 168.7(3).

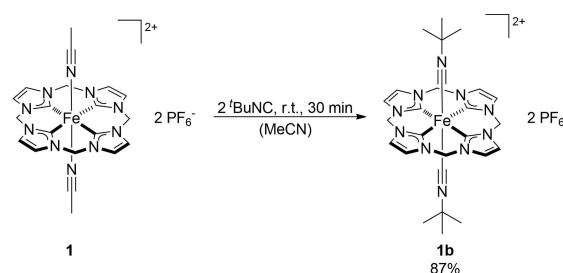
observed for **2** and its mono isocyanide substituted derivatives **2a–2d**, however it is more pronounced for **1** and **1a**.^[10]

Elemental analysis and ESI-MS are also in good accord with a composition of $[\text{Fe}(\text{cCCCC})(\text{CN}^t\text{Bu})(\text{MeCN})](\text{PF}_6)_2$.

Synthesis and characterisation of bis(*tert*-butylisocyanide) substituted iron(II) tetra-NHC **1b**

In contrast to **2**, when reacted with an excess of *tert*-butylisocyanide, **1** selectively forms bis(isocyanide) substituted complex **1b** (Scheme 2) instead of a tris(isocyanide) compound (**2f–2g**). This observation is mainly attributable to two factors. Firstly, the higher rigidity of the macrocyclic cCCCC ligand compared to open-chained NCCN impedes the substitution of one NHC moiety. Secondly, NHCs are considered as significantly stronger σ -donors than pyridines, thus making them less prone to ligand substitution.^[14]

The ^1H -NMR in acetone- d_6 of **1b** (Figure 2, bottom) displays a singlet with a chemical shift of 7.71 ppm and a relative integral of 8 assignable to the backbone protons. In comparison to **1** (7.57 ppm) the signal is significantly low field shifted (0.14 ppm) indicating a lower electron density of the iron centre, as already discussed for **1a** (see above). In contrast to **1a**, the methylene protons do not correspond to two doublets. Instead, they are referable to a singlet with a chemical shift of 6.46 ppm as a result of the higher symmetry of the bis(isocyanide) complex. The ^1H -NMR spectrum of **1b** recorded in CD_3CN (see SI, Figure 6) clearly shows two additional sets of signals which are not observed in deuterated acetone (see SI, Figure 5). In addition to the main signals clearly assignable to **1b**, equimolar amounts of about 7–8% (based on integral ratios) **1a** and free *tert*-butylisocyanide suggest that one isocyanide ligand is replaced in parts by the – in comparison to acetone – stronger coordinating solvent acetonitrile. The ^{13}C -NMR spectrum of **1b** in acetone- d_6 shows a signal at 196.1 ppm (see SI, Figure 7), which is in the typical range of iron(II) NHC complexes.^[8,10–11] As also observed for **1a**, the carbene resonance is significantly high-field shifted compared to compound **1** (205.1 ppm).^[8b] A similar influence of axial ligand substitution with a π -accepting carbonyl ligand, which is isolobal to *tert*-butylisocyanide,^[15] has been reported previously.^[8b] However, due the stronger π -acceptor property of CO the effect is more pronounced (179.3 ppm vs. 195.2 ppm). As discussed above, no



Scheme 2. Synthesis of bis(*tert*-butylisocyanide) substituted complex $[\text{Fe}(\text{cCCCC})(\text{CN}^t\text{Bu})_2](\text{PF}_6)_2$ **1b**.

resonance corresponding to the coordinating isocyanide carbon atom is observed in the ^{13}C -NMR spectrum.^[10,12]

In addition, **1b** was characterised by SC-XRD. Suitable single crystals were obtained by slow vapour diffusion of pentane into a solution of **1b** in acetone at room temperature. As expected, the complex exhibits a distorted octahedral coordination geometry (Figure 4).

The Fe–C_{carbene} distances of 1.894(4) Å to 1.903(4) Å are within range of other iron(II) NHC complexes and remain almost unchanged in comparison to the starting material **1** and mono(CN^tBu) complex **1a** (Figure 3).^[8,11,13] Both Fe–C_{isocyanide} distances of 1.861(4) Å and 1.876(4) Å are longer than that of mono-isocyanide complex **1a** (1.819(3) Å) suggesting a reduced backdonation from the iron(II) centre to the ligands which is a result of both π -acceptor ligands competing for backdonation. A similar observation is often reported for complexes bearing carbonyl ligands, which are isolobal to isocyanides.^[15–16] In alignment tris(isocyanide) complexes **2e–2h** also depict significantly longer Fe–C_{isocyanide} bonds than their mono substituted derivatives **2a–2d**.^[10] The considerably weaker Fe–C_{isocyanide} bond assigned by SC-XRD in **1b** compared to compound **1a** perfectly coincides with the observed partial dissociation in the

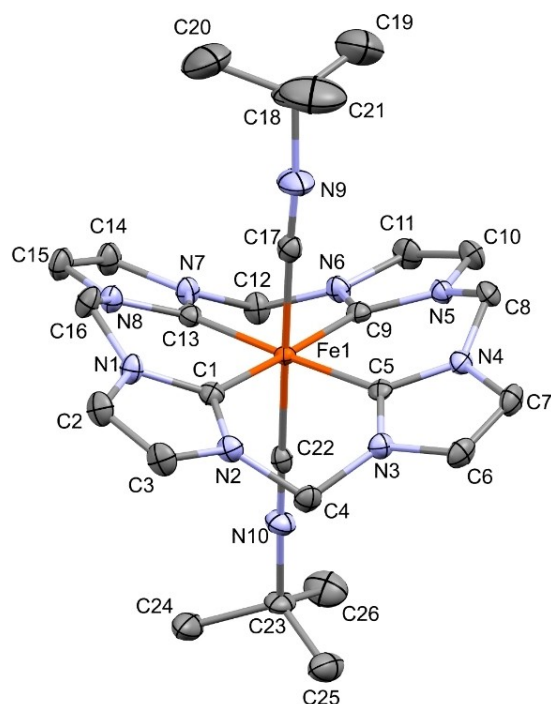


Figure 4. ORTEP-style representation of the cationic fragment of compound **1b**. Hydrogen atoms, co-crystallized solvent molecules and hexafluorophosphate anions are omitted for clarity. Thermal ellipsoids are shown at a 50% probability level. Selected bond lengths (Å) and angles (°): Fe1–C1 1.903(4), Fe1–C5 1.899(4), Fe1–C9 1.894(4), Fe1–C13 1.899(4), Fe1–C17 1.861(4), Fe1–C22 1.876(4), C17–Fe1–C5 90.59(15), C17–Fe1–C1 90.64(16), C5–Fe1–C1 90.34(16), C17–Fe1–C13 86.82(16), C5–Fe1–C13 177.40(15), C1–Fe1–C13 89.47(16), C17–Fe1–C9 86.78(15), C5–Fe1–C9 89.32(15), C1–Fe1–C9 177.39(11), C13–Fe1–C9 90.75(15), C17–Fe1–C22 176.44(16), C5–Fe1–C22 91.04(15), C1–Fe1–C22 92.52(15), C13–Fe1–C22 91.56(15), C9–Fe1–C22 90.07(15), N9–C17–Fe1 177.4(15), C17–N9–C18 173.2(16), N10–C22–Fe1 178.2(2), C22–N10–C23 179.1(4).

coordinating solvent acetonitrile (see above and SI, Figure 6), which does not occur for **1a**.

ESI-MS and elemental analysis are also in accord with a composition of $[\text{Fe}(\text{cCCCC})(\text{CN}^t\text{Bu})_2](\text{PF}_6)_2$.

Electrochemical investigations

In previous studies the electronic structure of iron(II) NHC complexes bearing tetradentate bis(pyridyl-NHC) ligand NCCN was reported to be significantly affected by the substitution of the labile acetonitrile ligands.^[10] Isocyanides are isolobal to CO and therefore exhibit a strong π -acceptor capability in addition to their σ -donor properties.^[15] However carbonyl ligands are considered to be better π -acceptors.^[15] As a result of isocyanide substitution a decreased electron density of the iron centre and therefore a higher potential for the oxidation of Fe(II) to Fe(III) is to be expected for the isocyanide substituted derivatives **1a** and **1b** in comparison to **1** bearing two axial MeCN ligands (Figure 1, left). In order to affirm this assumption, CV measurements of mono-substituted complex **1a** bearing one axial *tert*-butylisocyanide ligand, an isolobal analogue of mono(carbonyl) complex **1c**, were conducted to investigate the impact of the ligand substitution on the redox behaviour. Complex **1** with two axial MeCN ligands displays a reversible one-electron redox process with a half-cell potential of $E_{1/2} = 0.15$ V, which is assigned to the Fe(II)/Fe(III) redox couple (Figure 5, middle).^[8b] **1a** also shows a one-electron redox process assignable to the Fe(II)/Fe(III) redox couple (Figure 5, bottom), the reversibility of which indicates that no dissociation of the isocyanide ligand takes place after oxidation of the iron centre in contrast to some of the derivatives of **2** (Figure 1).^[10] As expected, the half-cell potential $E_{1/2} = 0.35$ of **1a** is significantly increased ($\Delta E_{1/2} = +0.20$ V) in comparison to **1**, confirming the assumption of a decrease in electron density at the iron centre caused by the axial *tert*-butylisocyanide π -acceptor ligand. In accordance with the better π -acceptor capability of CO in comparison to isocyanides,^{31, 32} **1c**, the isolobal carbonyl analogue of **1a**, displays an even higher half-cell potential ($E_{1/2} = 0.83$ V).^[8b]

Like **1** and **1a**, **1b** shows a one-electron redox peak assignable to the Fe(II)/Fe(III) redox couple (Figure 5, top; $E_{1/2} = 0.47$ V). The reversibility of the redox peak suggests that in contrast to tris(isocyanide) complexes **2e–2g** no ligand dissociation takes place as a result of the oxidation of the iron centre. As expected, the substitution with another π -accepting CN^tBu ligand results in a considerably more pronounced increase of the half-cell potential compared to mono(isocyanide) complex **1a** ($E_{1/2} = 0.35$ V) and bis(acetonitrile) compound **1** ($E_{1/2} = 0.15$ V).

The half-cell potential of **1b** ($E_{1/2} = 0.44$ V) is significantly lower in comparison to its carbonyl analogue **1d** ($E_{1/2} = 1.25$ V) bearing two better π -accepting *trans* axial CO ligands.^[8b,15]

The CV measurement of **1b** was conducted in acetonitrile for a better comparability to **1** and **1a**. As evidenced by ^1H -NMR spectroscopy (see above and SI, Figure 6), one CN^tBu ligand dissociates in small parts in acetonitrile. Therefore, another unincisive redox peak ($E_{1/2} = 0.35$ V) assignable to **1a** is

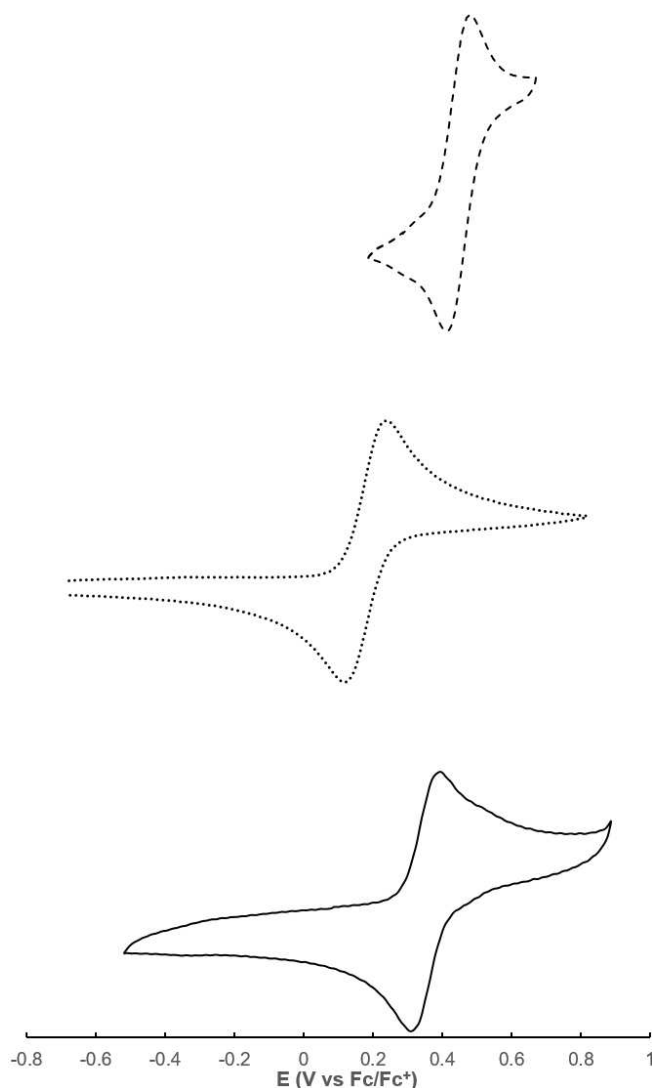


Figure 5. Cyclic voltammogram of compound **1a** in MeCN (bottom). Half-cell potential is determined to $E_{1/2} = 0.35$ V and oxidation/reduction potentials are determined to $E_{\text{ox}} = 0.39$ V and $E_{\text{red}} = 0.31$ V. Cyclic voltammogram of compound **1b** in MeCN (top). Half-cell potential is determined to $E_{1/2} = 0.47$ V and oxidation/reduction potentials are determined to $E_{\text{ox}} = 0.50$ V and $E_{\text{red}} = 0.44$ V. All potentials are given relative to the Fc/Fc^+ redox couple. Cyclic voltammogram of compound **1** in MeCN (middle). Half-cell potential is determined to $E_{1/2} = 0.15$ V and oxidation/reduction potentials are determined to $E_{\text{ox}} = 0.20$ V and $E_{\text{red}} = 0.11$ V.^[8b] All potentials are given relative to the Fc/Fc^+ redox couple.

observed in the cyclic voltammogram on closer inspection (Figure 5, top).

Conclusion

The reaction of iron(II) complex **1** bearing macrocyclic tetra-NHC ligand cCCCC and *trans* labile acetonitrile ligands with *tert*-butylisocyanide results in the selective formation of mono- or bis(isocyanide) substituted iron(II) complexes **1a** and **1b**, respectively, solely depending on the amount of isocyanide applied during synthesis. In contrast to compound **2**, the

reaction of **1** with an excess of isocyanide does not lead to the formation of a tris(isocyanide) compound as a result of the higher rigidity and stronger donating properties of the cCCCC ligand compared to bis(pyridyl-NHC) ligand NCCN. **1a** and **1b** are characterised by multinuclear NMR spectroscopy, ESI-MS, elemental analysis and SC-XRD. Mono(*tert*-butylisocyanide) complex **1a** shows a distorted octahedral geometry. The significantly stronger donating properties of cCCCC in comparison to NCCN induce a stronger π -backdonation from the iron centre to the isocyanide ligand indicated by a considerably shortened $\text{Fe}-\text{C}_{\text{isocyanide}}$ bond compared to mono(isocyanide) NCCN complexes **2a–2d**. As expected, the substitution of one acetonitrile ligand with the π -accepting *tert*-butylisocyanide increases the half-cell potential of the one electron $\text{Fe(II)}/\text{Fe(III)}$ redox step from $E_{1/2} = 0.15$ V to $E_{1/2} = 0.35$ V relative to the Fc/Fc^+ redox couple. The reversibility of the process indicates that no dissociation of the isocyanide ligand takes place after oxidation in contrast to some of the isocyanide derivatives of **2**. Like mono(*tert*-butylisocyanide) compound **1a**, bis(*tert*-butylisocyanide) compound **1b** also displays a distorted octahedral coordination geometry. In alignment with other complexes bearing multiple carbonyl ligands, both isolobal analogue *tert*-butylisocyanide ligands compete for backdonation from the iron(II) centre, resulting in a reduced mean π -backbonding and significantly longer $\text{Fe}-\text{C}_{\text{isocyanide}}$ distances compared to mono-isocyanide complex **1a**. In comparison to **1** ($E_{1/2} = 0.15$ V) and **1a** ($E_{1/2} = 0.35$ V), **1b** exhibits the highest half-cell potential assignable to the reversible $\text{Fe(II)}/\text{Fe(III)}$ redox process ($E_{1/2} = 0.44$ V), conforming with the lowest electron density of the iron centre caused by two axial π -acceptor ligands. As a result of the weaker $\text{Fe}-\text{C}_{\text{isocyanide}}$ bond in **1b** and as demonstrated by ^1H -NMR spectroscopy, a small amount of CN^tBu dissociates in the weakly coordinating solvent acetonitrile (7–8%) leading to an equilibrium with **1a** which is not observed in acetone. Therefore, another unincisive redox peak corresponding to **1a** is observed in the cyclic voltammogram of **1b** acquired in acetonitrile. These results demonstrate that axial ligand substitution is an effective method for the electronic fine-tuning of highly active olefin epoxidation catalyst **1**.

The rarely studied influence of labile ligand substitution of iron-based oxidation catalysts on their performance is currently investigated in order to gain further insights into the development of more sustainable and applicable catalysts. As the half-cell potential of **1a** and **1b** lies in between that of **1** and **2**, their catalytic activity is expected to also be in between. However, if **1a** and **1b** follow the trend of **2** and its isocyanide derivatives **2a–2h**, a beneficial increase of their turnover number compared to **1** is achieved.

Experimental Section

General Procedures and Analytical Methods

Unless otherwise stated, all manipulations were performed under an argon atmosphere using standard Schlenk and glovebox techniques. **1** was synthesized according to a literature procedure.^[8b] All other reagents were purchased from commercial

suppliers and used without further purification. NMR spectra were recorded on a Bruker Avance DPX 400 ($^1\text{H-NMR}$, 400.13 MHz; $^{13}\text{C-NMR}$, 100.53 MHz; $^{31}\text{P-NMR}$, 162 MHz) and chemical shifts are reported relative to the residual signal of the deuterated solvent.^[17] Elemental analyses (C/H/N) were obtained by the microanalytical laboratory at Technische Universität München. Electrospray ionization mass spectrometry (ESI-MS) data were acquired on a *Thermo Fisher Ultimate 3000*.

Single crystal X-ray diffraction

X-ray crystallographic data were collected on a single crystal x-ray diffractometer with the following setups: a CCD detector (Bruker APEX II, κ -CCD), a fine-focus sealed tube and a graphite monochromator using the APEX2 software package. The measurement used MoK_α radiation ($\lambda = 0.71073 \text{ \AA}$) and was performed on single crystals coated with perfluorinated ether. The crystal was fixed on top of a glass fiber and frozen under a stream of cold nitrogen. A matrix scan was used to determine the initial lattice parameters. Reflections were corrected for Lorentz and polarization effects, scan speed, and background using SAINT. Absorption corrections, including odd and even ordered spherical harmonics were performed using SADABS. Space group assignments were based upon systematic absences, E statistics, and successful refinement of the structures. Structures were solved by direct methods (SHELXS) with the aid of successive difference Fourier maps, and were refined against all data using SHELXL-2014 in conjunction with SHELXLE.^[18] Hydrogen atoms were calculated in ideal positions as follows: Methyl hydrogen atoms were refined as part of rigid rotating groups, with a C–H distance of 0.98 Å and $U_{\text{iso(H)}} = 1.5 U_{\text{eq(C)}}$. Other H atoms were placed in calculated positions and refined using a riding model, with methylene and aromatic C–H distances of 0.99 Å and 0.95 Å, respectively, other C–H distances of 1.00 Å and $U_{\text{iso(H)}} = 1.2 U_{\text{eq(C)}}$. Non-hydrogen atoms were refined with anisotropic displacement parameters. Full-matrix least-squares refinements were carried out by minimizing $\sum w(F_o^2 - F_c^2)^2$ with SHELXL weighting scheme.^[18a] Neutral atom scattering factors for all atoms and anomalous dispersion corrections for the non-hydrogen atoms were taken from *International Tables for Crystallography*. Images of the crystal structures were generated with Mercury.^[19] CCDC 1984573–1984574 contain the supplementary crystallographic data for this paper. These data can be obtained free of charge via www.ccdc.cam.ac.uk/data_request/cif, or by emailing data_request@ccdc.cam.ac.uk, or by contacting The Cambridge Crystallographic Data Centre, 12 Union Road, Cambridge CB2 1EZ, UK; fax: +44 1223 336033.

Cyclic voltammetry

CV measurements were recorded using a Metrohm Autolab potentiostat employing a gastight three-electrode cell under an argon atmosphere. A glassy carbon electrode was used as the working electrode and polished before each measurement. A graphite stick was used as the counter electrode. The potential was measured against Ag/AgCl (3.00 M KCl) with a scan rate of 100 mV/s and ferrocene was used as internal standard. Tetrabutylammonium hexafluorophosphate (100 mM in MeCN) was used as the electrolyte. The concentration of the complexes was about 2 mM.

Synthetic procedures

$[\text{Fe}(\text{C}(\text{CCCC})(\text{CN}^t\text{Bu})(\text{MeCN}))(\text{PF}_6)_2$ **1a**: *tert*-Butylisocyanide (33.0 μL , 0.40 mmol, 1.00 equiv.) is added to a solution of **1** (300 mg, 400 μmol , 1.00 equiv.) in 10 mL acetone while stirring. Within minutes, the yellow solution changes its colour to emerald green

and back to yellow. After stirring for 30 min at room temperature, 20 mL diethyl ether is added resulting in the formation of a yellow precipitate. The precipitate is washed three times with 10 mL diethyl ether. After drying *in vacuo* the product is obtained as air-stable, yellow powder (249 mg, 360 μmol , 90%). Single crystals suitable for SC-XRD were obtained by slow vapour diffusion of Et_2O into a solution of **1a** in MeCN at room temperature. $^1\text{H-NMR}$ (400.13 MHz, acetone- d_6): δ 7.75 (s, 8H, CH_{im}), 6.60 (d, $^2J = 12.6 \text{ Hz}$, 4H, CH_2), 6.48 (d, $^2J = 12.6 \text{ Hz}$, 4H, CH_2), 1.88 (s, 3H, CH_3CN), 0.97 (s, 9H, $\text{C}(\text{CH}_3)_3$). $^{13}\text{C-NMR}$ $\{^1\text{H}\}$ (100.53 MHz, acetone- d_6): δ 198.9 ($\text{C}_{\text{Carbene}}$), 122.8 (CH_{im}), 63.3 (CH_2), 30.7 ($\text{C}(\text{CH}_3)_3$), 3.3 (CH_3CN). $^{31}\text{P-NMR}$ (162 MHz, acetone- d_6): δ -144.60 (hept, $^1J = 706.6 \text{ Hz}$). Anal. calcd. for $\text{C}_{23}\text{H}_{28}\text{F}_{12}\text{FeN}_{10}\text{P}_2$: C, 34.95; H, 3.57; N, 17.72. Found C, 35.17; H, 3.72; N, 17.42. MS-ESI (m/z): [**1a** - MeCN - PF_6^-] calcd., 605.13; found, 605.01; [**1a** - MeCN - 2PF_6^-] calcd., 230.08; found, 229.91.

$[\text{Fe}(\text{C}(\text{CCCC})(\text{CN}^t\text{Bu}))_2](\text{PF}_6)_2$ **1b**: *tert*-Butylisocyanide (152.0 μL , 1.20 mmol, 4.00 equiv.) is added to a solution of **1** (300 mg, 400 μmol , 1.00 equiv.) in 8 mL acetonitrile while stirring. Immediately after addition, the yellow solution changes its colour to emerald green. After stirring at room temperature for 30 min 20 mL diethyl ether is added resulting in the formation of a pale green precipitate. The precipitate is washed three times with 10 mL diethyl ether. After drying *in vacuo* the product is obtained as air-stable, pale green powder (290 mg, 349 μmol , 87%). Single crystals suitable for SC-XRD were obtained by slow vapour diffusion of pentane into a solution of **1b** in acetone at room temperature. $^1\text{H-NMR}$ (400.13 MHz, acetone- d_6): δ 7.71 (s, 8H, CH_{im}), 6.46 (s, 8H, CH_2), 1.09 (s, 18H, $\text{C}(\text{CH}_3)_3$). $^1\text{H-NMR}$ (400.13 MHz, CD_3CN): δ 7.44 (s, 8H, CH_{im}), 6.07 (s, 8H, CH_{im}), 1.01 (s, 18H, CH_{im}). $^{13}\text{C-NMR}$ $\{^1\text{H}\}$ (100.53 MHz, acetone- d_6): δ 196.1 ($\text{C}_{\text{Carbene}}$), 122.9 (CH_{im}), 63.2 (CH_2), 30.6 ($\text{C}(\text{CH}_3)_3$). $^{13}\text{C-NMR}$ $\{^1\text{H}\}$ (100.53 MHz, CD_3CN): δ 196.1 ($\text{C}_{\text{Carbene}}$), 122.8 (CH_{im}), 63.2 (CH_2), 30.4 ($\text{C}(\text{CH}_3)_3$). $^{31}\text{P-NMR}$ (162 MHz, acetone- d_6): δ -144.60 (hept, $^1J = 706.7 \text{ Hz}$). Anal. calcd. for $\text{C}_{26}\text{H}_{34}\text{F}_{12}\text{FeN}_{10}\text{P}_2$: C, 37.52; H, 4.12; N, 16.83. Found C, 37.46; H, 4.11; N, 16.96. MS-ESI (m/z): [**1b** - PF_6^-] calcd., 689.21; found, 689.30; [**1b** - 2PF_6^-] calcd., 272.12; found, 272.08.

Acknowledgements

The authors gratefully acknowledge support by the TUM graduate school. Benjamin J. Hofmann and Lukas Niederegger are acknowledged for support with the CV measurements. Christian Jandl is acknowledged for support with SC-XRD. Open access funding enabled and organized by Projekt DEAL.

Conflict of Interest

The authors declare no conflict of interest.

Keywords: non-heme iron complexes · *N*-heterocyclic carbene · electronic finetuning · cyclic voltammetry · isocyanide

- [1] J. W. Kück, M. R. Anneser, B. Hofmann, A. Pöthig, M. Cokoja, F. E. Kühn, *ChemSusChem* **2015**, *8*, 4056–4063.
[2] a) K. Riener, S. Haslinger, A. Raba, M. P. Högerl, M. Cokoja, W. A. Herrmann, F. E. Kühn, *Chem. Rev.* **2014**, *114*, 5215–5272; b) I. Bauer, H.-J. Knölker, *Chem. Rev.* **2015**, *115*, 3170–3387; c) S. Enthaler, K. Junge, M. Beller, *Angew. Chem. Int. Ed.* **2008**, *47*, 3317–3321; d) K. Gopalaiah, *Chem. Rev.* **2013**, *113*, 3248–3296.

- [3] C. Bolm, J. Legros, J. Le Pailh, L. Zani, *Chem. Rev.* **2004**, *104*, 6217–6254.
- [4] E. C. Theil, D. J. Goss, *Chem. Rev.* **2009**, *109*, 4568–4579.
- [5] a) M. Costas, M. P. Mehn, M. P. Jensen, L. Que, *Chem. Rev.* **2004**, *104*, 939–986; b) S. M. Hölzl, P. J. Altmann, J. W. Kück, F. E. Kühn, *Coord. Chem. Rev.* **2017**, *352*, 517–536; c) K. P. Bryliakov, E. P. Talsi, *Coord. Chem. Rev.* **2014**, *276*, 73–96; d) Y. O. R. W. Nam, W. J. Song, *J. Biol. Inorg. Chem.* **2004**, *9*.
- [6] a) L. Que Jr, W. B. Tolman, *Nature* **2008**, *455*, 333; b) A. B. McQuarters, M. W. Wolf, A. P. Hunt, N. Lehnert, *Angew. Chem. Int. Ed.* **2014**, *53*, 4750–4752.
- [7] a) M. N. Hopkinson, C. Richter, M. Schedler, F. Glorius, *Nature* **2014**, *510*, 485–496; b) D. J. Nelson, *Eur. J. Inorg. Chem.* **2015**, *2015*, 2012–2027; c) L.-A. Schaper, S. J. Hock, W. A. Herrmann, F. E. Kühn, *Angew. Chem. Int. Ed.* **2013**, *52*, 270–289; d) F. E. Hahn, M. C. Jahnke, *Angew. Chem. Int. Ed.* **2008**, *47*, 3122–3172.
- [8] a) A. Raba, M. Cokoja, S. Ewald, K. Riener, E. Herdtweck, A. Pöthig, W. A. Herrmann, F. E. Kühn, *Organometallics* **2012**, *31*, 2793–2800; b) M. R. Anneser, S. Haslinger, A. Pöthig, M. Cokoja, J.-M. Basset, F. E. Kühn, *Inorg. Chem.* **2015**, *54*, 3797–3804; c) J. F. Schlagintweit, F. Dyckhoff, L. Nguyen, C. H. G. Jakob, R. M. Reich, F. E. Kühn, *J. Catal.* **2020**, *383*, 144–152.
- [9] a) J. W. Kück, A. Raba, I. I. E. Markovits, M. Cokoja, F. E. Kühn, *ChemCatChem* **2014**, *6*, 1882–1886; b) A. C. Lindhorst, J. Schütz, T. Netscher, W. Bonrath, F. E. Kühn, *Catal. Sci. Technol.* **2017**, *7*, 1902–1911.
- [10] S. Haslinger, A. C. Lindhorst, J. W. Kück, M. Cokoja, A. Pöthig, F. E. Kühn, *RSC Adv.* **2015**, *5*, 85486–85493.
- [11] I. Klawitter, M. R. Anneser, S. Dechert, S. Meyer, S. Demeshko, S. Haslinger, A. Pöthig, F. E. Kühn, F. Meyer, *Organometallics* **2015**, *34*, 2819–2825.
- [12] R. W. Stephany, M. J. A. de Bie, W. Drenth, *Org. Magn. Reson.* **1974**, *6*, 45–47.
- [13] a) S. A. Cramer, D. M. Jenkins, *J. Am. Chem. Soc.* **2011**, *133*, 19342–19345; b) M. R. Anneser, G. R. Elpitiya, X. B. Powers, D. M. Jenkins, *Organometallics* **2019**, *38*, 981–987.
- [14] a) K. Denk, P. Sirsch, W. A. Herrmann, *J. Organomet. Chem.* **2002**, *649*, 219–224; b) W. A. Herrmann, M. Elison, J. Fischer, C. Köcher, G. R. J. Artus, *Chem. Eur. J.* **1996**, *2*, 772–780; c) B. T. Heaton, C. Jacob, J. T. Sampanthar, *J. Chem. Soc. Dalton Trans.* **1998**, 1403–1410; d) J. Slattery, R. J. Thatcher, Q. Shi, R. E. Douthwaite, *Pure Appl. Chem.* **2010**, *82*, 1663–1671.
- [15] a) F. A. Cotton, F. Zingales, *J. Am. Chem. Soc.* **1961**, *83*, 351–355; b) I. P. Csonka, L. Szepes, A. Modelli, *J. Mass Spectrom.* **2004**, *39*, 1456–1466; c) L. Weber, *Angew. Chem. Int. Ed.* **1998**, *37*, 1515–1517; d) Y. Yamamoto, *Coord. Chem. Rev.* **1980**, *32*, 193–233.
- [16] P. Kamer, D. Vogt, J. W. Thybaut, *Contemporary catalysis: science, technology, and applications*, Royal Society Of Chemistry, Cambridge, **2017**.
- [17] G. R. Fulmer, A. J. M. Miller, N. H. Sherden, H. E. Gottlieb, A. Nudelman, B. M. Stoltz, J. E. Bercaw, K. I. Goldberg, *Organometallics* **2010**, *29*, 2176–2179.
- [18] a) G. Sheldrick, *Acta Crystallogr. Sect. C* **2015**, *71*, 3–8; b) C. B. Hubschle, G. M. Sheldrick, B. Dittrich, *J. Appl. Crystallogr.* **2011**, *44*, 1281–1284.
- [19] C. F. Macrae, I. J. Bruno, J. A. Chisholm, P. R. Edgington, P. McCabe, E. Pidcock, L. Rodriguez-Monge, R. Taylor, J. van de Streek, P. A. Wood, *J. Appl. Crystallogr.* **2008**, *41*, 466–470.

Manuscript received: February 20, 2020

Revised manuscript received: March 22, 2020

Version of record online: April 2, 2020